Dalton Transactions

c6dt04253h

1

Bipyridine based metallogels: an unprecedented difference in photochemical and chemical reduction in the *in situ* nanoparticle formation

Rajendhraprasad Tatikonda, Kia Bertula, Nonappa, Sami Hietala, Kari Rissanen* and Matti Haukka*

Reduction of silver containing metallogels led to formation of silver nanoparticles (AgNP's). Considerable size and morphological differences of the AgNP's were observed between the standard chemical and photochemical reduction of the metallogels.

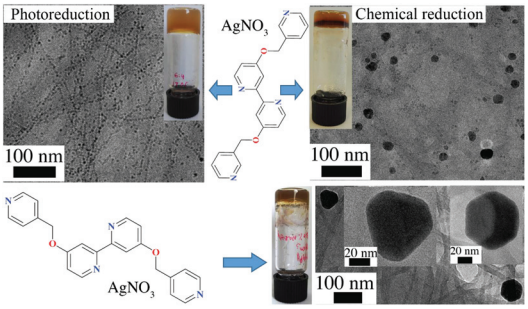

Please check this proof carefully. **Our staff will not read it in detail after you have returned it.**

Translation errors between word-processor files and typesetting systems can occur so the whole proof needs to be read. Please pay particular attention to: tabulated material; equations; numerical data; figures and graphics; and references. If you have not already indicated the corresponding author(s) please mark their name(s) with an asterisk. Please e-mail a list of corrections or the PDF with electronic notes attached – do not change the text within the PDF file or send a revised manuscript. Corrections at this stage should be minor and not involve extensive changes. All corrections must be sent at the same time.

Please bear in mind that minor layout improvements, e.g. in line breaking, table widths and graphic placement, are routinely applied to the final version.

We will publish articles on the web as soon as possible after receiving your corrections; **no late corrections will be made**.

Please return your **final** corrections, where possible within **48 hours** of receipt, by e-mail to: dalton@rsc.org

Queries for the attention of the authors

Journal: **Dalton Transactions**

Paper: **c6dt04253h**

Title: **Bipyridine based metallogels: an unprecedented difference in photochemical and chemical reduction in the *in situ* nanoparticle formation**

Editor's queries are marked like this [Q1, Q2, ...], and for your convenience line numbers are indicated like this [5, 10, 15, ...].

Please ensure that all queries are answered when returning your proof corrections so that publication of your article is not delayed.

Query Reference	Query	Remarks
Q1	For your information: You can cite this article before you receive notification of the page numbers by using the following format: (authors), Dalton Trans., (year), DOI: 10.1039/c6dt04253h.	
Q2	Please check that the inserted CCDC numbers are correct.	
Q3	Please carefully check the spelling of all author names. This is important for the correct indexing and future citation of your article. No late corrections can be made.	
Q4	Ref. 8*b*: Can this reference be updated?	
Q5	Please check that ref. 9*b* has been displayed correctly.	
Q6	Ref. 13*a*, 13*c*–*g*, 17, 39*b*–*e* and 41*a*: Please provide the initials for Nonappa.	

Dalton Transactions

PAPER

Bipyridine based metallogels: an unprecedented difference in photochemical and chemical reduction in the *in situ* nanoparticle formation†

Cite this: DOI: 10.1039/c6dt04253h

Rajendhraprasad Tatikonda,[a] Kia Bertula,[b] Nonappa,[b] Sami Hietala,[c] Kari Rissanen*[a] and Matti Haukka*[a]

Received 8th November 2016,
Accepted 2nd February 2017

DOI: 10.1039/c6dt04253h

rsc.li/dalton

Metal co-ordination induced supramolecular gelation of low molecular weight organic ligands is a rapidly expanding area of research due to the potential in creating hierarchically self-assembled multi-stimuli responsive materials. In this context, structurally simple *O*-methylpyridine derivatives of 4,4′-dihydroxy-2,2′-bipyridine ligands are reported. Upon complexation with Ag(I) ions in aqueous dimethyl sulfoxide (DMSO) solutions the ligands spontaneously form metallosupramolecular gels at concentrations as low as 0.6 w/v%. The metal ions induce the self-assembly of three dimensional (3D) fibrillar networks followed by the spontaneous *in situ* reduction of the Ag-centers to silver nanoparticles (AgNPs) when exposed to daylight. Significant size and morphological differences of the AgNP's was observed between the standard chemical and photochemical reduction of the metallogels. The gelation ability, the nanoparticle formation and rheological properties were found to be depend on the ligand structure, while the strength of the gels is affected by the water content of the gels.

Introduction

Metallosupramolecular chemistry offers control over self-assembly from molecular, nanoscale to mesoscale superstructures with multiple stimuli and functionalities.[1] Among supramolecular self-assembled systems, the hierarchical assembly of low molecular weight building blocks ranging from morphologically diverse nano- and micrometer structures to hydro- and organogelation is a topical and highly attractive area of research.[2] The ability of structurally simple building blocks to generate highly entangled three dimensional (3D) fibrillar networks and encapsulation of solvents provides potential applications in the field of tissue engineering,[3] separations,[4] biomedicine,[5] optoelectronics,[6] catalysis,[7] chiral plasmonics,[8] *in situ* nanoparticle formation,[9] and templating of porous/hollow inorganic nanotubes.[10] Molecular building blocks used, *viz.* low molecular weight gelators (LMWG), range from simple heteroatom containing hydrocarbons[11] to peptides,[12] steroids,[13] nucleobases,[14] carbohydrates,[15] polyaromatics[16] and alkaloids,[17] all of which have been extensively been studied as gel forming agents. The gelator molecules are able to utilize one or several supramolecular interactions such as H-bonding, electrostatic interactions, π-stacking, van der Waals interaction, charge transfer complexation, halogen bonding, fluorine–fluorine interactions and dynamic covalent bonds in the gel formation.[18] Metal complexation has been extensively studied in the field of supramolecular self-assembly to generate molecular, supramolecular and nanoscopic structures.[19] Recently, the metal chelation induced aggregation of low molecular weight organic ligands has been extended to hydro- and organogelation, now known as metallogels or metallosupramolecular gels.[18d,20] In order to obtain metallogels, at least one of the above mentioned supramolecular interactions is needed in addition to metal coordination. Therefore, gelators containing metal binding sites (ligands) such as pyridine, bipyridine, terpyrdines and carboxylates, have been utilized as the core of the metallogelator.[21] Examples include cholesterol derivatives, dendrimers, oligopeptides and oligoethylene glycol derivatives.[22] Recently, subcomponent self-assembly,[22] has been used as a facile route for metallogels.[23] The bipyridine derivatives have been studied for their ability to form supramolecular gels upon complexation with metal ions such as Fe(II), Co(II), Ni(II), Cu(II), Zn(II) and

[a]Department of Chemistry, Nanoscience Center, University of Jyväskylä, P. O. Box 35, FI-40014 Jyväskylä, Finland. E-mail: matti.o.haukka@jyu.fi, kari.t.rissanen@jyu.fi
[b]Department of Applied Physics, Molecular Materials Group, Aalto University School of Science, Puumiehenkuja 2, FI-02150 Espoo, Finland
[c]Department of Chemistry, Department of Chemistry, University of Helsinki, P. O. Box 55, FI-00014 Helsinki, Finland

†Electronic supplementary information (ESI) available: General methods and materials, single crystal X-ray data, ^{1}H, ^{13}C and 2D NMR spectra of ligands 2–4 and its complexes, additional SEM and TEM micrographs. CCDC 1500637–1500639. For ESI and crystallographic data in CIF or other electronic format see DOI: 10.1039/c6dt04253h

Ag(I).[24] The formed metal complex can induce or disrupt the gelation and even act as precursor for *in situ* nanoparticle formation.[25,26] Because of their antibacterial properties the polymeric as well as low molecular weight hybrid gels containing silver nanoparticles (AgNP) have gained considerable interest.[27] Typically this type of gels are synthesized by using sodium borohydride mediated chemical reduction,[28] photochemical reduction,[29] microwave irradiation,[30] sonochemical reduction,[31] or by using ascorbic acid and glucose as reducing agents.[32] It has been demonstrated that the size of AgNPs are dependent on the ratio of metal ion to the capping agent and the strength of the reducing agent.[31] Silver nanoparticles are sensitive to light and atmospheric oxygen, therefore proper capping agents and stabilizers are needed to prevent the aggregation. Furthermore, it has been shown that photo-irradiation using appropriate source of light in the presence of photochemical reducing agents AgNPs can be obtained without using additional stabilizers.[33] *In situ* AgNP formation upon standing the pyridyl containing bis(urea) based hybrid gels have been reported, where in the formation of AgNPs was accelerated using UV irradiation.[34] Similarly, oligo(*p*-phenylvinylene) based metallogels have been reported to act as templates for AgNP formation.[35] The photochemical deposition of AgNPs on helical fibers based on unsymmetrical triphenylene derivatives containing imidazole moieties have been carried out by using UV irradiation. It has been shown that in this case the nanoparticle formation is dependent on the structural isomers of imidazole moieties.[36] In majority of hybrid gels the nanoparticles were stabilized by the gelator/gel fibers and no external capping agents were necessary.[37] Even though, extensive research on *in situ* chemical reduction as well as photo-irradiation mediated reduction of nanoparticles in supramolecular gels have been reported, a comparison of simple daylight mediated AgNP formation with chemical reduction in the same gel has not been pursued extensively. In this context, we report Ag(I) induced self-assembly of synthetically simple 4,4′-bis(pyridinylmethoxy)-2,2′-bipyridine derivatives in aqueous dimethyl sulfoxide to supramolecular gels. We demonstrate that the metal complexation not only furnishes self-assembled fibrillar networks (SAFINs), but also acts as a precursor for the *in situ* silver nanoparticle formation within the gel matrix *via* photochemical reduction upon exposure to daylight. A remarkable size and morphological differences between standard chemical reduction and the photochemical daylight reduction was observed. While the gelation itself and the nanoparticle formation upon reduction of the gel depends on the structure of the gelator, the rheological properties are affected by the water content of the gel as well as the counter anions. More importantly, unlike many metallogelators, the gelators presented in this work lack the conventional hydrogen bonding moieties. The structures of the ligands, complexes, gels and xerogels are characterized using NMR spectroscopy (1D and 2D), single crystal X-ray diffraction, electron microscopy and rheological measurements.

Results and discussion

The bipyridyl ligands were prepared upon reacting 4,4′-dihydroxy-2,2′-bipyridine **1**, with 2-, 3-, or 4-chloromethyl pyridine hydrochloride in the presence of potassium carbonate (K_2CO_3) resulting in ligands **2**, **3** or **4** (Scheme 1), respectively. The solid materials obtained after purification were used for further studies. Ligands **2**, **3** and **4** resulted in single crystals upon recrystallization from chloroform (ESI†).[38] Fig. 1a–c

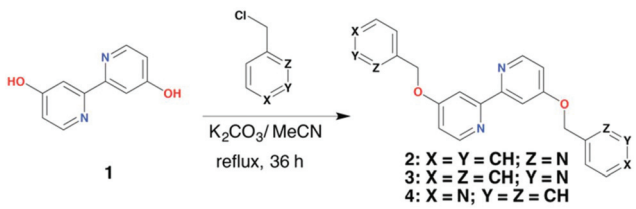

Scheme 1 Synthesis and chemical structures of ligands **2**–**4**.

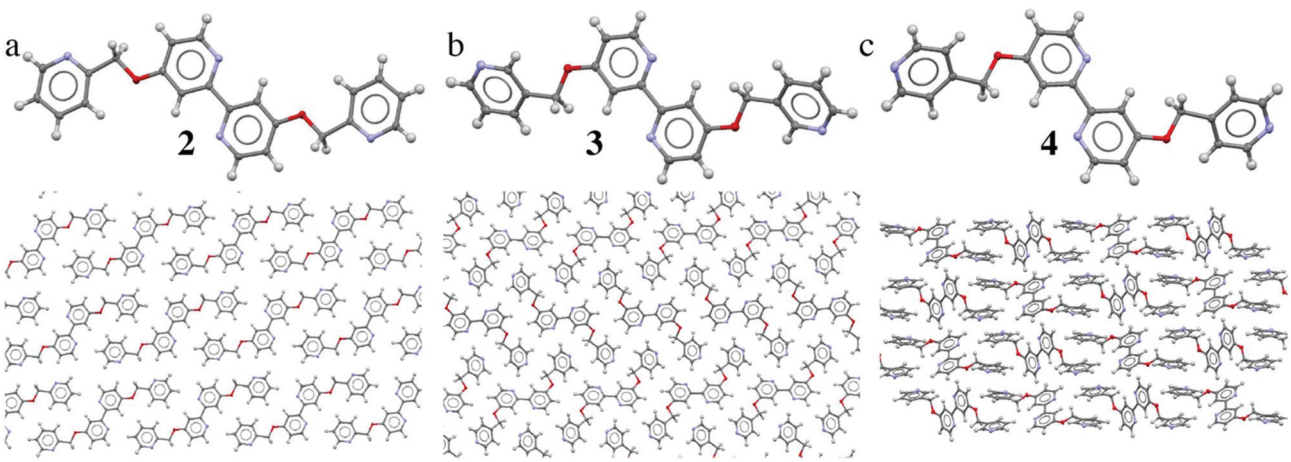

Fig. 1 Single crystal X-ray studies. Single crystal X-ray structures and packing patterns of ligands (a) **2**, (b) **3** and (c) **4**.

shows the single crystal X-ray structures as well as unit cell packing of ligands **2**, **3** and **4**, respectively.

The ligands **2** and **3** crystallized in triclinic space group $P\bar{1}$ and ligand **4** in monoclinic space group $P2_1/c$ (see ESI, Table S1 and Fig. S1–S3†). A systematic analysis of the crystal packing of ligand **2**, **3** and **4** reveals that **2** has weak C═C–H···N and CH_2···N hydrogen bonding to the pyridine nitrogens, while **4** shows only C═C–H···N to pyridine nitrogens. Contrary to **2** and **4**, the ligand **3** exhibits weak C═C–H···N and CH_2···N hydrogen bonding to both bipyridine and pyridine nitrogens. In addition to these weak hydrogen bonds, the packing commences through off-set π···π interactions for **2** and **4** (3.5 Å in both structures), while the ligand **3** shows the face-to-face π···π interactions at slightly longer distance (3.6 Å) (Fig. 1a–c).

The ligands were then studied for metal complexation by dissolving them in DMSO by heating, followed by addition of equimolar $AgNO_3$ as water solution, creating a dimethyl sulfoxide : water (DMSO : H_2O) solvent system. Ligand **2** upon complexation with $AgNO_3$ forms [**2·AgNO$_3$**] which precipitates out of the solution as a powder. Whereas the addition of aqueous $AgNO_3$ to a solution of ligands **3** and **4** resulted in an instantaneous gelation (Fig. 2 and 3) and stable gels were obtained after heating the mixture to obtain a clear solution followed by allowing the sol to attain room temperature. However, when the similar tests were performed for ligands without any metal ions, ligand **3** resulted in an unstable gel, which collapsed upon standing at room temperature for several hours. Ligand **4** produced only precipitate (see ESI Fig. S4†) due to the formation of microcrystalline aggregates as revealed by scanning electron microscopy (SEM) imaging (Fig. 2a and b). To confirm the role of the metal we performed further studies on metallogels. Gelation tests with $CuCl_2$, $ZnCl_2$, $CdCl_2$, $HgCl_2$ and $HAuCl_4$ produced only precipitates and no metallogels were obtained (ESI, Table S2†). This suggests that the gelation is cation specific.

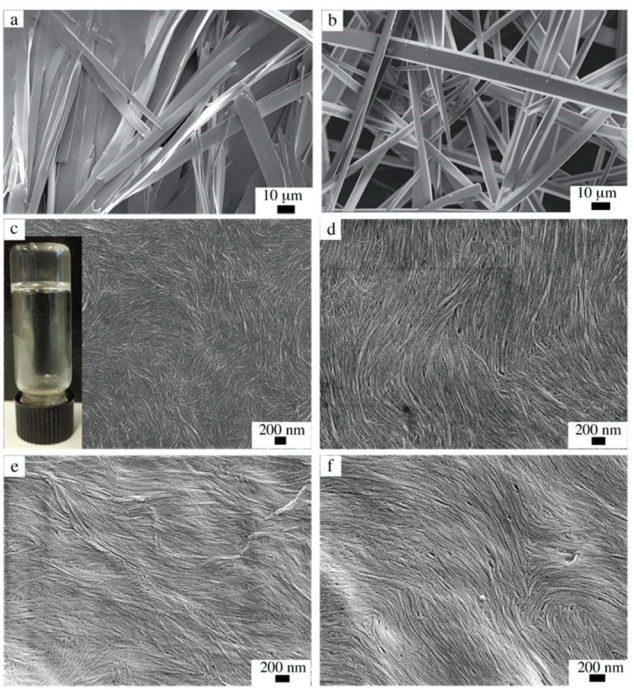

Fig. 2 SEM micrographs of xerogels derived from 0.6 w/v% of (a) ligand **3**; (b) ligand **4**, [**3·AgNO$_3$**] at different v/v DMSO/H_2O ratio (c) 8 : 2; (d) 7 : 3; (e) 6 : 4 and (f) 1 : 1.

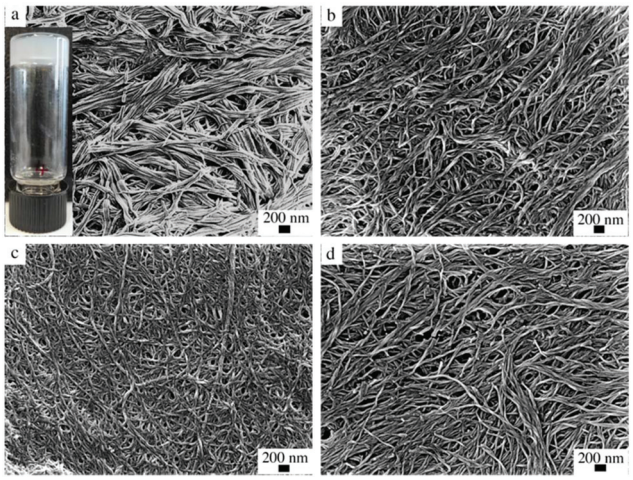

Fig. 3 SEM micrographs of xerogels derived from 0.6 w/v% [**4·AgNO$_3$**] at different v/v DMSO/H_2O ratio. (a) 8 : 2; (b) 7 : 3; (c) 6 : 4 and (d) 1 : 1.

The gelation was observed at various DMSO : H_2O (v/v) ratios and in this study four different ratios were used, *viz.* 8 : 2, 7 : 3, 6 : 4 and 1 : 1. The gels obtained are either transparent or translucent depending on the ratio of DMSO : H_2O used for gelation. As there is no gelation with the ligand **2** upon Ag(I) complexation but a precipitate formation, the importance of nitrogen atom position in the pyridine ring becomes crucial for the gelation. The structural information and the morphological features of the self-assembled fibrillar metallogel networks in the DMSO : H_2O gels [**3·AgNO$_3$**] and [**4·AgNO$_3$**] were studied using scanning electron microscopy, SEM (see ESI† for details). Fig. 2 shows the SEM micrographs of the dried gels (xerogels) of [**3·AgNO$_3$**] upon drying under ambient conditions at different v/v ratio of DMSO : H_2O.

The presence of the very fine/thin nanofibrillar networks formed upon gelation is evident from SEM micrographs and the nature of the fibers does not display any significant changes upon changing the ratio of solvents. However, increasing the water content resulted in more translucent gels. The [**4·AgNO$_3$**] gels showed more robust/thick highly entangled nanofibers under SEM analysis (Fig. 3). The morphological features remained similar in different solvent ratio. The metallogelation was also observed in DMF : H_2O system. However, dissolving the precipitate formed upon complexation by heating resulted in an immediate dark brown coloured gel. It is attributed to the rapid reduction of silver ions (see ESI†) by DMF, which is well documented in the literature. Importantly, the morphological features of the xerogels were found to be similar to that of DMSO : H_2O gels.

The mechanical properties of the [**3**·$AgNO_3$] and [**4**·$AgNO_3$] gels were studied using rheological measurements (Fig. 4). Accordingly, time sweep and frequency sweep experiments using freshly prepared gels were performed. The gels showed characteristic features of viscoelastic solids as the storage moduli G′ was higher than the loss moduli G″ for gels derived from both the ligands. Interestingly, the [**4**·$AgNO_3$] gels are somewhat stronger than that of [**3**·$AgNO_3$] (Fig. 4). Fig. 4a and b shows the storage (G′) and loss moduli G″ of [**3**·$AgNO_3$] and [**4**·$AgNO_3$]. The [**3**·$AgNO_3$] gels with elastic modulus G′ of 100 Pa, showed no significant change upon changing the DMSO/H_2O ratio. However, [**4**·$AgNO_3$] gels showed higher G′ values (800–1000 Pa) compared to that of [**3**·$AgNO_3$] gels at 8 : 2 DMSO : H_2O ratio. Unlike [**3**·$AgNO_3$] gels, a significant change in the gel strength was observed upon changing the DMSO : H_2O ratio. The gels at 8 : 2 and 7 : 2 ratio display similar G′ values (800–1000 Pa). However, G′ values for 6 : 4 and 1 : 1 gels dropped by almost four times compared to that of 8 : 2 and 7 : 3 gels. The difference observed in the gel strength between [**3**·$AgNO_3$] and [**4**·$AgNO_3$] gels can be attributed to the difference in morphological features of two gels. The scanning electron micrograph of gels also shows a clear difference in the fibrillar networks formed during gelation. The [**3**·$AgNO_3$] gels have the tendency to form fine, more film-like, structures upon casting over substrate (Fig. 2), while those of [**4**·$AgNO_3$] clearly show thicker nanofibrillar networks (Fig. 3).

Gelation was also observed when the complexation of ligand **3** and **4** was performed with other counter anions of silver(I) such as PF_6, BF_4, ClO_4, OAc, CF_3SO_3. Stable metallogels were obtained with all counter anions of silver(I) when ligand **3** was used (see ESI, Table S3 and Fig. S7†). However, gels obtained with ligand **4** were less stable and most of them collapsed after a few hours at room temperature. SEM micrographs revealed the formation of entangled fibrillar networks

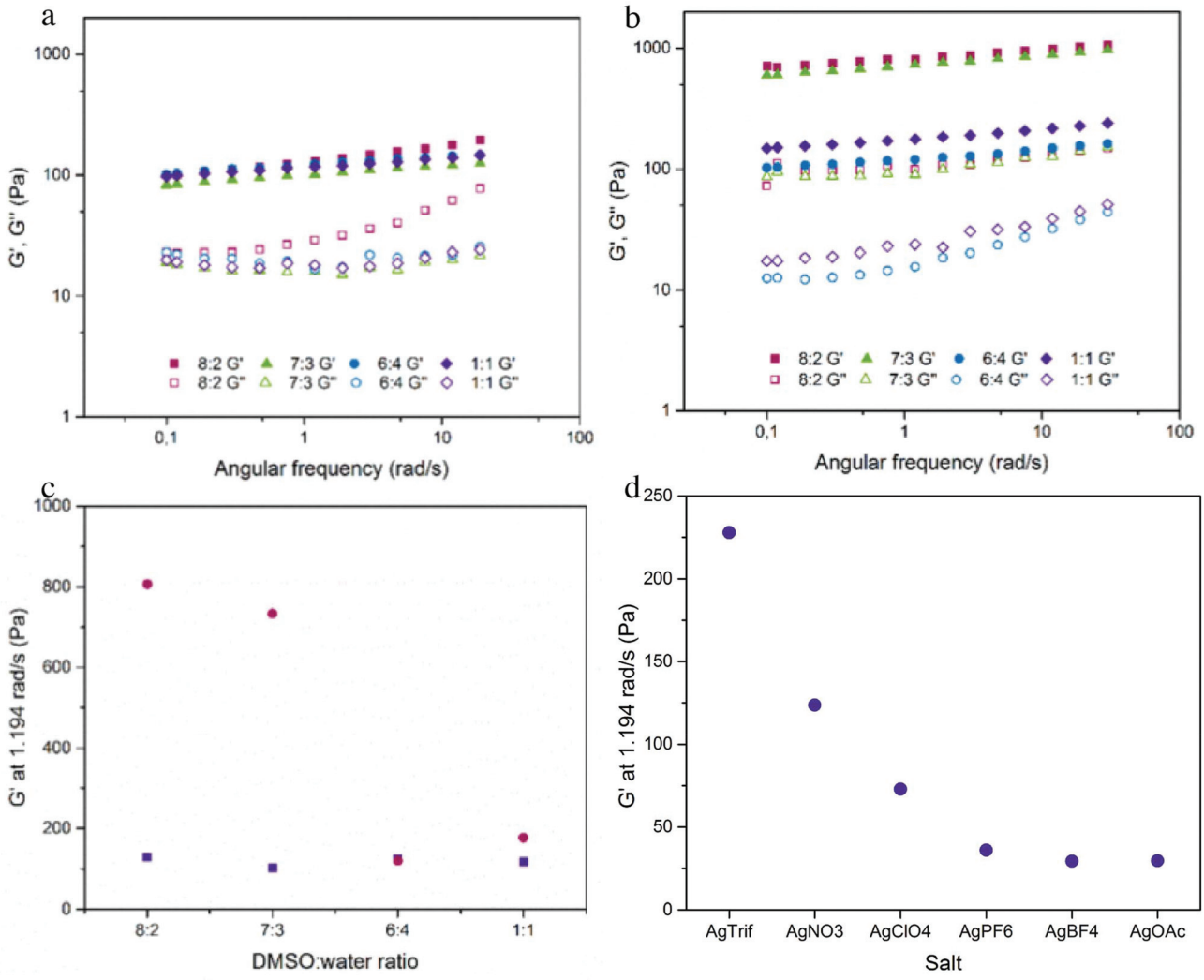

Fig. 4 Rheological properties. (a) Frequency sweep experiments for 0.6 w/v% DMSO/H_2O gels of [**3**·$AgNO_3$]; (b) frequency sweep experiments for DMSO/H_2O gels of [**4**·$AgNO_3$]; (c) storage modulus G′ as a function of DMSO/H_2O ratio of [**3**·$AgNO_3$]; (purple square) and [**4**·$AgNO_3$]; (red circle) and (d) shows the effect of counter anions on the mechanical properties of metallogels derived from ligand **3**.

similar to those obtained using $AgNO_3$ metallogels (see ESI Fig. S8 and S9†). The anions have a significant effect on the mechanical property of the gels as revealed by rheological measurements (see ESI Fig. S10†). The strength of the gel varies in the order $CF_3SO_3 > NO_3 > ClO_4 > PF_6 > BF_4 \cong OAc$ (Fig. 4d).

NMR spectroscopic studies of the conventional and metallogels have been done both in solution and in the solid state to gain more detailed information about the mode of intermolecular interactions, for determination the gel melting temperatures, gelation kinetics and packing modes of the gel states.[39] In this work, one dimensional (1D) ^1H, ^{13}C NMR spectroscopy as well as two dimensional (2D) ^1H–^1H correlation spectroscopy (COSY), ^1H–^{13}C heteronuclear multiple quantum correlation (HMQC) and ^1H–^{15}N COSY were performed for **2**, **3** and **4** and their Ag-complexes (see ESI Fig. S11–S20†). The assignment of resonance peaks arising from ^1H and ^{13}C and their correlation allows monitoring the changes that occur during metal coordination. The ligands **2–4** used in this study, unlike many gelator molecules reported in the literature lack the hydrogen bonding ability. Therefore, the weak supramolecular interactions very likely enhanced by the nitrate anions between metallopolymer chains lead to the formation of the nanofibrillar networks (see below) and are thus the major driving forces for the gel formation. The Ag-cation coordinates to the nitrogen atoms of the ligands and thus affects the α-protons to the coordination site allowing the comparison of metal complexes. Fig. 5a shows the ^1H NMR spectra of ligand **3** and its 1 : 1 metal complex, [**3·AgNO$_3$**], in pure DMSO-d_6 (see ESI Fig. S18 and S19† for ligands **2** and **4** as well as their Ag(I) complexes).

Upon metal complexation, a significant change in the chemical shifts for all the protons was observed. A systematic analysis of ^1H NMR spectrum of [**3·AgNO$_3$**] showed that the protons adjacent to the nitrogen atoms (H1, H5 and H6) are 0.07–0.04 ppm downfield shifted compare to that of the free ligand. Similarly, the protons H7 and H8 showed a similar downfield shift (0.07 ppm) upon complexation. However, relatively large and significant changes in the chemical shift values were observed for protons H3 and H2 (0.13 and 0.2 ppm respectively). The proton signals of the ligands move downfield due to the deshielding effect of the metal coordination. A similar behaviour was also observed for the ^{13}C signals (see ESI, Fig. S20†). The Ag-complexation clearly affects all the protons of the ligand and indicates that all the four nitrogens, both in the bipyridine and pyridine moieties are involved in metal complexation. To probe it further 2D ^1H–^{15}N correlation spectroscopy in DMSO-d_6 for free ligand and its complexes was done. Fig. 5b and c show the ^1H–^{15}N 2D correlation spectra of the free ligand **3** and the 1 : 1 metal complex [**3·AgNO$_3$**], respectively.

Upon complexation, clear changes in the chemical shift value of nitrogen atoms was observed. The nitrogen atoms of the bipyridine moiety (N1) showed an upfield shift of 24.91 ppm, while the pyridine nitrogens (N2) were shifted by 5.65 ppm (Fig. 5b). This supports the ^1H NMR observation that

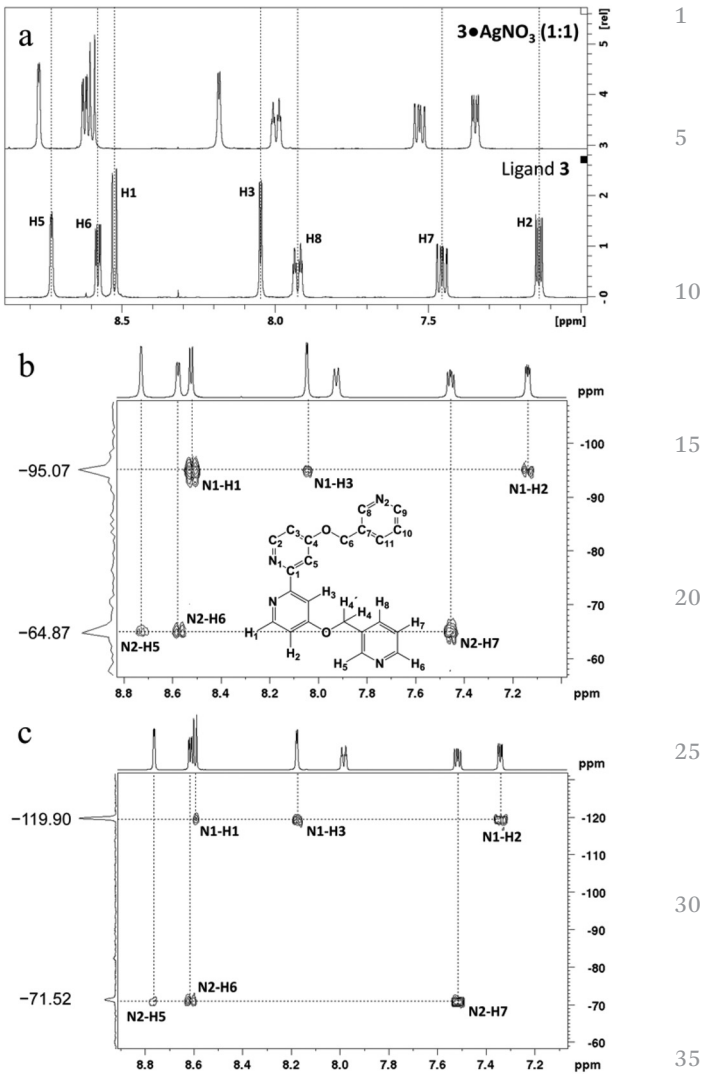

Fig. 5 The ^1H NMR spectra of ligand **3** and [**3·AgNO$_3$**] (a), ^1H–^{15}N 2D correlation spectrum of ligand **3** (b) and ^1H–^{15}N 2D correlation spectrum of ligand [**3·AgNO$_3$**] (c) in DMSO-d_6 at 30 °C.

all nitrogen atoms of the ligand are involved in the metal coordination. The most common Ag^+ coordination geometry is tetrahedral, especially with bipyridine and pyridine ligands.[40]

Based on the 1 : 1 ratio of the ligand and the $AgNO_3$, and the NMR spectral analysis (Fig. 5) and MM-level Spartan® molecular modelling (see ESI, Fig. S22–S24†), the structure of the $AgNO_3$ complex is a metallopolymer, where the silver cation is tetrahedrally coordinated one bipyridine unit and to a pyridine nitrogen of two adjacent ligands (Fig. 6). To support this, gelation studies performed using 1 : 2 ligand to metal ratio resulted in crystallization of the excess silver nitrate, indicating that all the four nitrogen atoms of ligand are involved in coordination in the 1 : 1 ratio complex.

Thermal behaviour of the [**3·AgNO$_3$**] gel in DMSO-d_6/D_2O was probed by variable temperature (VT) ^1H NMR experiments from 30 °C–90 °C with 10 °C increments (see ESI Fig. S21†). The gels showed characteristic broad signals at room tempera-

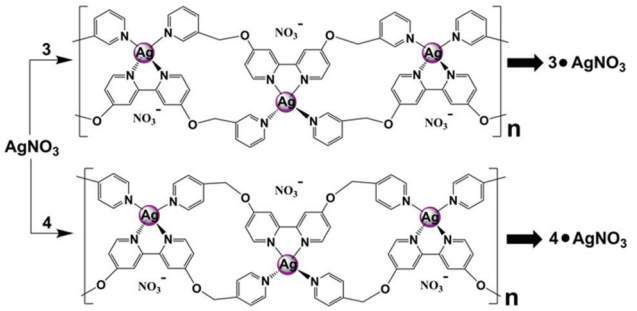

Fig. 6 The proposed structure of the metallosupramolecular polymer [3·AgNO$_3$] and [4·AgNO$_3$]. The MM-level molecular modeling of [3·AgNO$_3$] and [4·AgNO$_3$], see ESI.†

ture and line sharpening was observed upon increasing the temperature. However, due to high thermal stability of the gels the complete gel–sol transition was not reached as the gels remained stable even at high temperatures. Therefore, both gel melting and extensive VT NMR experiments were not performed. Investigations using FT-IR spectroscopic experiments showed a significant shift in the C=C, C=N stretching frequencies between the ligands and the complexes (see ESI Fig. S25 and S26†). In detail, FT-IR spectra of pure ligands, ligand xerogels and the xerogels obtained from the metallogels were compared. The peaks at 1558 and 1565 cm^{-1} of the ligand **3** shifted to 1565 and 1600 cm^{-1} for [**3·AgNO$_3$**]. Similarly, for ligand **4**, the stretching frequencies 1561 and 1568 cm^{-1} shifted to 1562 cm^{-1} and 1601 cm^{-1} respectively for [**4·AgNO$_3$**].

Unprecedentedly upon exposing the [**3·AgNO$_3$**] gels to daylight, a gradual color change from colorless transparent gel to pale brown was observed. Fig. 7 shows the visual color change in [**3·AgNO$_3$**] gel after 14 days of daylight exposure. However, the [**4·AgNO$_3$**] gels this colour change was very weak. The [**3·AgNO$_3$**] gel network remained stable for months after the daylight reduction, this might be due to the gelation ability of ligand **3** without silver in similar conditions. It may also indicate that only part of silver(I) ions reduced forming nanoparticles. The color change turned out to be result from the daylight induced reduction of the silver ions into silver nanoparticles. Nanoparticle formation was confirmed by using UV-Vis spectroscopy with characteristic surface plasmon resonance around 430 nm (Fig. 7b, see ESI Fig. S27†).[41]

Detailed morphological analysis was done using transmission electron microscopy (TEM). The TEM micrographs revealed highly entangled fibrillar networks in both [**3·AgNO$_3$**] and [**4·AgNO$_3$**] gels (ESI†). Fig. 8a and b show the TEM images of the *in situ* formed AgNP's over gel network under daylight reduction for [**3·AgNO$_3$**] gel. Highly monodisperse AgNP's with a diameter of 3–4 nm arrays were formed on the gel network fibres under daylight reduction (See Fig. S25–S28† for additional TEM micrographs). To compare these photochemically obtained *in situ* nanoparticles, we conducted a standard sodium borohydride reduction of the [**3·AgNO$_3$**] gel (see ESI†

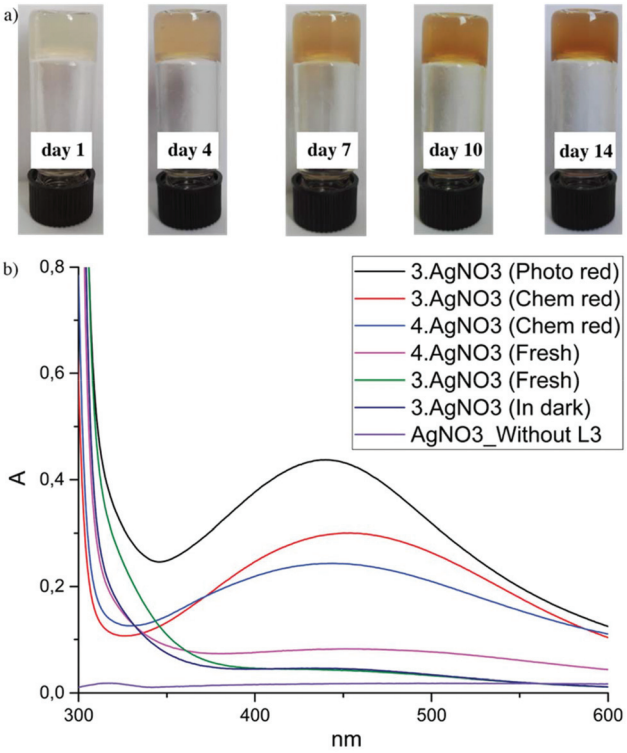

Fig. 7 (a) Photographs showing colour change of 0.6 w/v% DMSO/H$_2$O gel of [**3·AgNO$_3$**] upon exposure to daylight. (b) UV-vis spectra of freshly prepared, daylight reduced, chemically reduced metallogels in DMSO and control samples.

for experimental details). To our surprise the chemical reduction resulted in quite polydisperse and much larger AgNP's (*ca.* 20–25 nm in diameter, Fig. 8c and d) scattered quite uniformly across the gel matrix, not situated on the network fibres. The results are in agreement with the UV-Vis spectroscopy, which shows a broad surface plasmon resonance peak around 450 nm (Fig. 7b).

To probe what happen with the photochemically inactive [**4·AgNO$_3$**] gels a similar sodium borohydride reduction was done (see ESI† for experimental details). The TEM micrographs from the AgNP's from the [**4·AgNO$_3$**] were very symmetrical, either cuboctahedron or prismatic in shape, and much larger (>50 nm) (Fig. 8e and f). The above results suggest that the molecular structure of the ligands not only affect the strength and morphological features of the gel network but also on the *in situ* nanoparticle formation. The TEM micrographs obtained from freshly prepared gels in DMF : H$_2$O showed the random aggregates of silver nanoparticles (see ESI Fig. S35†). A control experiment using a solution of AgNO$_3$ in DMSO : H$_2$O upon exposing for daylight for one week remained unchanged without any color change. Similarly, freshly prepared [**3·AgNO$_3$**] gel upon storing under dark remained colorless for one week and no plasmon resonance was observed in UV-Vis spectra (Fig. 7b). The above results further supporting the importance of daylight mediated *in situ* nanoparticle formation.

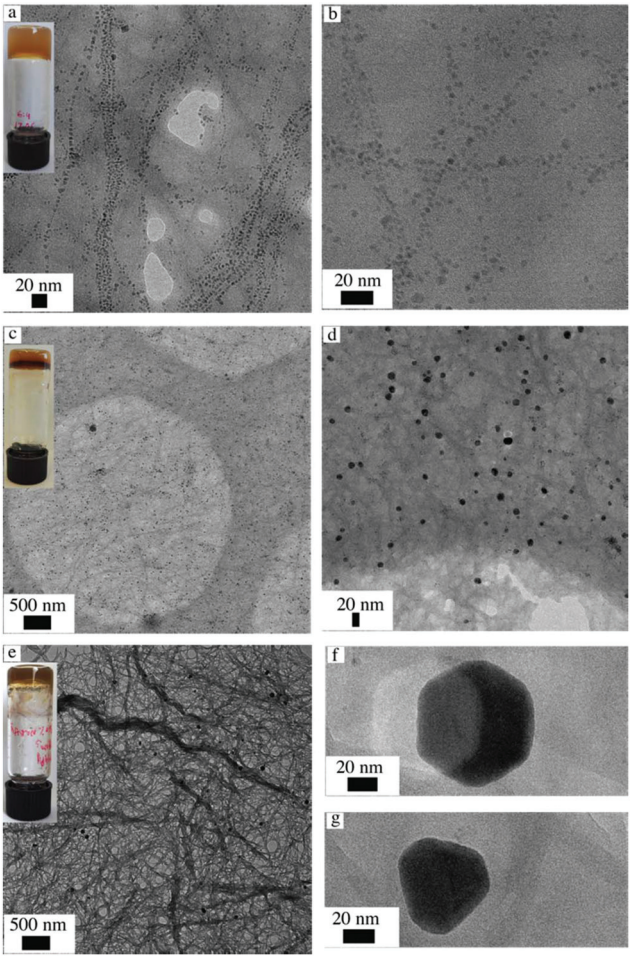

Fig. 8 *In situ* nanoparticle formation. TEM micrographs of (a & b) photochemically reduced [**3·AgNO$_3$**] gel upon exposure to daylight; (c & d) $NaBH_4$ mediated chemically reduced [**3·AgNO$_3$**] gel; (e) chemically reduced [**4·AgNO$_3$**] gel and (f & g) shows cuboctohedron and prismatic nanoparticles respectively from [**4·AgNO$_3$**] gel.

Conclusions

We have shown that simple bipyridyl based ligands are able to act as supergelators upon complexation with silver ions. The gels are formed at a concentration as low as 0.6 w/v% in aqueous dimethyl sulfoxide. The gelation ability, morphological features and mechanical properties strongly depends on the ligand molecular structure. More importantly, the metal coordination not only induces gel formation but also act as a precursor for *in situ* silver nanoparticle formation. The significant differences between chemical and daylight induced *in situ* nanoparticle formation for the [**3·AgNO$_3$**] gel result in from the morphology of the nanofibrillar networks of the gels and also the structure of the metallopolymer responsible for the gelation. In addition the differences in the size and morphology of the AgNP's from the chemical reduction of [**3·AgNO$_3$**] and [**4·AgNO$_3$**] gel highlights the importance of accessibility of the reducing agent to the metal center of the metallopolymers. This, in turn, is greatly affected by structure of the metallopolymer. The discovery that in the [**3·AgNO$_3$**] gel the photochemical reduction of the Ag-centers produced AgNP's embedded in the fibres of the gel matrix with narrow size distribution was a totally unexpected result. Recently, there is a growing interesting in developing methods to control nanoparticles with well-defined size and shape, as they possess unique self-assembling abilities as well as material properties. Therefore, our findings become relevant both in molecular gels and nanoparticle synthesis. Such a finding can pave a way to new soft photoactive materials, which are responsive to daylight.

Experimental section

General procedure for the synthesis of ligands 2, 3 and 4

A mixture of 4,4′-dihydroxy-2,2′-bipyridine (188.2 mg, 1 mmol), potassium carbonate, K_2CO_3 (276.5 mg, 2 mmol) in 30 mL of acetonitrile was stirred at room temperature for 2 h. 2- or 3- or 4-(chloromethyl) pyridine hydrochloride (328.1 mg, 2 mmol) was added to the above mixture and heated to reflux for 36 h. After the reaction time, the filtrate was collected by filtration and evaporated to dryness. The product was recrystallized from MeOH and dried under vacuum.

4,4′-Bis(pyridin-2-ylmethoxy)-2,2′-bipyridine (2). ^{1}H NMR (400 MHz, $CDCl_3$) δ 8.63 (dq, 1H), 8.51 (d, 1H), 8.50 (d, 1H), 8.10 (d, 1H), 7.73 (td, 1H), 7.52 (dt, 1H), 7.25 (m, 1H), 6.93 (dd, 1H), 5.35 (s, 2H). ^{13}C NMR (100 MHz, $CDCl_3$) δ = 165.77, 157.98, 156.23, 150.64, 149.66, 137.15, 123.16, 121.64, 111.21, 107.96, 70.71.

^{1}H NMR (500 MHz, DMSO-d_6 at 70 °C) δ 8.59 (dq, 1H), 8.50 (d, 1H), 8.01 (d, 1H), 7.84 (dt, 1H), 7.55 (d, 1H), 7.35 (qd, 1H), 7.11 (dd, 1H), 5.36 (s, 2H). ^{1}H–^{15}N COSY NMR (DMSO-d_6 at 70 °C) δ = −68.12 (pyridine) and −94.41 (bipy).

4,4′-Bis(pyridin-3-ylmethoxy)-2,2′-bipyridine (3). ^{1}H NMR (400 MHz, $CDCl_3$) δ = 8.71 (d, 1H), 8.61 (dd, 1H), 8.50 (d, 1H), 8.10 (d, 1H), 7.79 (dt, 1H), 7.34 (dd, 1H), 6.91 (dd, 1H), 5.24 (s, 2H). ^{13}C NMR (100 MHz, $CDCl_3$) δ 165.66, 157.99, 150.54, 150.00, 149.25, 135.56, 131.61, 123.79, 111.81, 107.01, 67.62.

^{1}H NMR (500 MHz, DMSO-d_6) δ 8.73 (d, 1H), 8.58 (dd, 1H), 8.52 (d, 1H), 8.05 (d, 1H), 7.92 (dt, 1H), 7.45 (qd, 1H), 7.14 (dd, 1H), 5.35 (s, 2H). ^{13}C NMR (100 MHz, DMSO-d_6) δ 165.15, 150.62, 149.41, 149.17, 135.84, 131.79, 123.67, 111.42, 106.74, 67.07. ^{1}H–^{15}N COSY NMR (DMSO-d_6 at 30 °C) δ = −64.87 (pyridine) and −95.07 (bipy).

4,4′-Bis(pyridin-4-ylmethoxy)-2,2′-bipyridine (4). ^{1}H NMR (400 MHz, $CDCl_3$) δ 8.65 (dd, 2H), 8.51 (d, 1H), 8.08 (d, 1H), 7.38 (d, 2H), 6.93 (dd, 1H), 5.26 (s, 2H). ^{13}C NMR (100 MHz, $CDCl_3$) δ 165.61, 157.79, 150.52, 150.34, 145.09, 121.69, 111.83, 107.25, 68.20.

^{1}H NMR (500 MHz, DMSO-d_6 at 70 °C) δ 8.60 (dd, 2H), 8.51 (d, 1H), 8.02 (d, 1H), 7.47(d, 2H), 7.11 (dd, 1H), 5.37 (s, 2H). ^{1}H–^{15}N COSY NMR (DMSO-d_6 at 70 °C) δ = −65.35 (pyridine) and −94.18 (bipy).

Metal complexes

[**2·AgNO$_3$**]: ^{1}H NMR (500 MHz, DMSO-d_6) δ 8.62 (dq, 1H), 8.54 (d, 1H), 8.05 (d, 1H), 7.88 (dt, 1H), 7.59 (d, 1H), 7.39 (qd,

1H), 7.22 (dd, 1H), 5.42 (s, 2H). ^{1}H–^{15}N COSY NMR (DMSO-d_6 at 70 °C) δ = −71.01 (pyridine) and −112.41 (bipy).

[**3·AgNO$_3$**]: ^{1}H NMR (500 MHz, DMSO-d_6) δ 8.77 (d, 1H), 8.62 (dd, 1H), 8.59 (d, 1H), 8.18 (d, 1H), 7.99 (dt, 1H), 7.52 (qd, 1H), 7.34 (dd, 1H), 5.44 (s, 2H). ^{13}C NMR (100 MHz, DMSO-d_6) δ 166.10, 153.85, 151.92, 149.95, 149.63, 136.49, 131.66, 123.98, 112.03, 109.60, 67.67. ^{1}H–^{15}N COSY NMR (DMSO-d_6 at 30 °C) δ = −71.52 (pyridine) and −119.98 (bipy).

[**4·AgNO$_3$**]: ^{1}H NMR (500 MHz, DMSO-d_6) δ 8.63 (dd, 2H), 8.57 (d, 1H), 8.09 (d, 1H), 7.51 (d, 2H), 7.25 (dd, 1H), 5.44 (s, 2H). ^{1}H–^{15}N COSY NMR (DMSO-d_6 at 70 °C) δ = −69.32 (pyridine) and −107.53 (bipy).

General procedure for metallogelation

In a typical gelation experiment, the appropriate amounts of solid ligand (**3** or **4**) is placed in a test tube (45 × 15 mm) and dissolved in DMSO upon heating, whereupon equimolar amount of $AgNO_3$ solution in water is added to reach the final volume of 1.0 mL. The mixture is then heated to obtain a clear solution which, as it cooled down to room temperature, would afford a translucent gel. The gelation was observed at various ratios of DMSO/H_2O (v/v) and in this study four different ratios were used, *viz.* 8 : 2, 7 : 3, 6 : 4 and 1 : 1. No gels were obtained by using DMSO only.

Only ligand **3** forms unstable gel in an aqueous DMSO solvent at 1 wt%. No gelation was observed for ligand **4**.

Chemical reduction

In chemical reduction, the gel (**3·AgNO$_3$** or **4·AgNO$_3$**) was reduced from aqueous solution of $NaBH_4$. 1.0 mL of $NaBH_4$ solution which is 20 wt% to the silver molar amount in the gel was placed on the top of the gel and allowed it for slow diffusion at room temperature. During this time, $NaBH_4$ was diffused into the gel and reduces Ag^+ to Ag^0. In [**3·AgNO$_3$**] gel, the complete reduction was observed in a week period and in [**4·AgNO$_3$**] gel the reduction was slower and takes about 3 weeks. At high wt% of $NaBH_4$ (more than 40 wt% of $NaBH_4$) the reduction was faster and gel network was collapsed.

X-ray crystallography

Single crystal X-ray structure determination: the single crystals of ligands **2–4** were obtained by slow evaporation of chloroform solution. The X-ray diffraction data were collected on an Agilent Technologies Supernova diffractometer using Mo Kα or Cu Kα radiation. The CrysAlisPro program packages were used for cell refinements and data reductions. Structures were solved by charge flipping method using SUPERFLIP program or by direct methods using SHELXS-2008 program. Gaussian absorption correction was applied to all data and structural refinements were carried out using SHELXL-2015 software.

Scanning electron microscopy (SEM)

The sample preparation for SEM was performed by dissolving 6 mg of ligand (**3** or **4**) in 800 μL of DMSO with heating, to this clear solution equimolar amount of $AgNO_3$ in 200 μL of water was added. The resulting precipitate was solubilized by heating and let it cool down to room temperature to get a gel. The gel was then heated until it turned into a clear solution and drop casted over a carbon tape placed over aluminium stub. The sample was then allowed to dry under ambient conditions subjected from sputter coating with Au under vacuum conditions at 20 mA for 1 min. The samples were then subjected for imaging with Sigma Zeiss scanning electron microscope.

Rheological measurements

TA AR2000 stress controlled rheometer equipped with 20 mm steel plate and a Peltier heated plate was used for rheological characterization. The measuring setup was covered with a sealing lid in order to prevent evaporation during the measurements. Measurements were performed using oscillation frequency of 6.284 rad s^{-1} at 20 °C unless otherwise noted.

Transmission electron microscopy (TEM)

The transmission electron microscopy (TEM) images were collected using FEI Tecnai G2 operated at 120 kV and JEM 3200FSC field emission microscope (JEOL) operated at 300 kV in bright field mode with Omega-type Zero-loss energy filter. The images were acquired with GATAN DIGITAL MICROGRAPH software while the specimen temperature was maintained at −187 °C. The TEM samples were prepared by placing 3–5 μL of the pre-made gel on to a 300 mesh copper grid with holey carbon support film. The samples were dried under ambient condition prior to imaging.

Acknowledgements

T. R. and M. H. kindly acknowledge the financial support from the Academy of Finland (M. H. Proj. no. 295581, K. R. Proj. no. 263256, 265328, and 292746). Academy Professor Olli Ikkala, Aalto University, Finland is kindly acknowledged for financial support through the Academy of Finland, Centre of Excellence in Molecular Engineering of Biosynthetic Hybrid Materials (HYBER, 2014–2019) and ERC advanced grant (ERC-2011-AdG-291364) MIMEFUN (postdoc grant to Nonappa). The Aalto University Nanomicroscopy Center (Aalto-NMC) is kindly acknowledged for the use of its facilities. EU COST action CM 1302 "Smart Inorganic Polymers" is also gratefully acknowledged.

References

1 (*a*) S. J. Dalgarno, N. P. Power and J. L. Atwood, *Coord. Chem. Rev.*, 2008, **252**, 825–841; (*b*) B. H. Northrop, Y.-R. Zheng, K.-W. Chi and P. J. Stang, *Acc. Chem. Res.*, 2009, **42**, 1554–1563.

2 (*a*) R. G. Weiss and P. Terech, *Molecular Gels: Materials with self-assembled fibrillar, networks*, Springer, Dordrecht, The Netherlands, 2006; (*b*) A. R. Hirst, B. Escuder, J. F. Miravet

and D. K. Smith, *Angew. Chem., Int. Ed.*, 2008, **47**, 8002–8018.

3 J. Yan, B. S. Wong and L. Kang, Molecular Gels for Tissue Engineering, in *Soft fibrillar materials: Fabrication and applications*, ed. X. Y. Liu and J.-L. Li, Wiley-VCH Verlag GmbH & Co. KGaA, Weinheim, Germany, 2013, pp. 129–162.

4 C. K. Karan and M. Bhattacharjee, *Appl. Mater. Interfaces*, 2016, **8**, 5526–5535.

5 (*a*) P. K. Vemula, J. Li and G. John, *J. Am. Chem. Soc.*, 2006, **128**, 8932–8938; (*b*) E. Busseron, Y. Ruff, E. Moulin and N. Giuseppone, *Nanoscale*, 2013, **5**, 7098–7140; (*c*) R. Dong, Y. Pang, Y. Su and X. Zhu, *Biomater. Sci.*, 2015, **3**, 937–954.

6 (*a*) L. Korala, Z. Wang, Y. Liu, S. Maldonado and S. L. Brock, *ACS Nano*, 2013, **7**, 1215–1223; (*b*) S. Nardecchia, D. Carriazo, M. L. Ferrer, M. C. Gutierrez and F. del Monte, *Chem. Soc. Rev.*, 2013, **42**, 794–830; (*c*) J. D. Tovar, *Acc. Chem. Res.*, 2013, **46**, 1527–1537.

7 (*a*) J. F. Miravet and B. Escuder, *Chem. Commun.*, 2005, 5796–5798; (*b*) J. Potier, S. Menuel, M.-H. Chambrier, L. Burylo, J.-F. Blach, P. Woisel, E. Monflier and F. Hapiot, *Catal.*, 2013, **3**, 1618–1621.

8 (*a*) S. H. Jung, J. Jeon, H. Kim, J. Jaworski and J. H. Jung, *J. Am. Chem. Soc.*, 2014, **136**, 6446–6452; (*b*) X. Lan and Q. Wang, *Adv. Mater.*, 2016, DOI: 10.1002/adma.201600697.

9 (*a*) S. Ray, A. K. Das and A. Banerjee, *Chem. Commun.*, 2006, 2816–2818; (*b*) Z. X. Liu, Y. Feng, Z. Y. Zhao, Z. C. Yan, Y. M. He, X. J. Luo, C. Y. Liu and Q. H. Fan, *Chem. – Eur. J.*, 2014, **20**, 533–541; B. O. Okesola, S. K. Suravaram, A. Parkin and D. K. Smith, *Angew. Chem., Int. Ed.*, 2016, **128**, 191–195.

10 J. H. Jung and S. Shinkai, *Top. Curr. Chem.*, 2004, **248**, 223–260.

11 D. J. Abdallah, L. Lu and R. G. Weiss, *Chem. Mater.*, 1999, **11**, 2907.

12 (*a*) C. Tomasini and N. Castellucci, *Chem. Soc. Rev.*, 2013, **42**, 156–172; (*b*) S. Federico, U. Nöchel, C. Löwenberg, A. Lendlein and A. T. Neffe, *Acta Biomater.*, 2016, **38**, 1–10; (*c*) F. Xie, L. Qin and M. Liu, *Chem. Commun.*, 2016, **52**, 930–933; (*d*) M. Tena-Solsona, J. Nanda, S. Diaz-Oltra, A. Chotera, G. Ashkenasy and B. Escuder, *Chem. – Eur. J.*, 2016, **22**, 6687–6694.

13 (*a*) Nonappa and U. Maitra, *Org. Biomol. Chem.*, 2008, **6**, 657–669; (*b*) S. Banerjee, V. M. Vidya, A. J. Savyasachi and U. Maitra, *J. Mater. Chem.*, 2011, **21**, 14693–14705; (*c*) H. Svobodova, Nonappa, Z. Wimmer and E. Kolehmainen, *J. Colloid Interface Sci.*, 2011, **361**, 587–593; (*d*) S. Ikonen, Nonappa and E. Kolehmainen, *CrystEngComm*, 2010, **12**, 4304–4311; (*e*) S. Ikonen, Nonappa, A. Valkonen, R. Juvonen, H. Salo and E. Kolehmainen, *Org. Biomol. Chem.*, 2010, **8**, 2784–2794; (*f*) Nonappa and U. Maitra, *Soft Matter*, 2007, **3**, 1428–1433; (*g*) T. T. T. Myllymäki, Nonappa, H. Yang, V. Liljeström, M. A. Kostiainen, J.-M. Malho, X. X. Zhu and O. Ikkala, *Soft Matter*, 2016, **12**, 7159–7165.

14 (*a*) I. Yoshikawa, S. Yanagi, Y. Yamaji and K. Araki, *Tetrahedron*, 2007, **63**, 7474–7481; (*b*) Z. Yang, P.-L. Ho, G. Liang, K. H. Chow, Q. Wang, Y. Cao, Z. Guo and B. Xu, *J. Am. Chem. Soc.*, 2007, **129**, 266–267; (*c*) G. Godeau and P. Barthelemy, *Langmuir*, 2009, **25**, 8447–8450; (*d*) G. M. Peters and J. T. Davis, *Chem. Soc. Rev.*, 2016, **45**, 3188–3206.

15 (*a*) R. J. H. Hafkamp, M. C. Feiters and R. J. M. Nolte, *J. Org. Chem.*, 1999, **64**, 412–426; (*b*) N. Yan, G. He, H. Zhang, L. Ding and Y. Fang, *Langmuir*, 2010, **26**, 5909–5917; (*c*) Y. Ogawa, C. Yoshiyama and T. Kitaoka, *Langmuir*, 2012, **28**, 4404–4412.

16 (*a*) D. Rizkov, J. Gun, O. Lev, R. Sicsic and A. Melman, *Langmuir*, 2005, **21**, 12130–12138; (*b*) P. Mukhopadhyay, Y. Iwashita, M. Shirakawa, S. Kawano, N. Fujita and S. Shinkai, *Angew. Chem., Int. Ed.*, 2006, **45**, 1592–1595; (*c*) D. Singh and J. B. Baruah, *Tetrahedron Lett.*, 2008, **49**, 4374–4377.

17 Nonappa and E. Kolehmainen, *Gels*, 2016, **2**, 9.

18 (*a*) M. Suzuki, Y. Nakajima, M. Yumoto, M. Kimura, H. Shirai and K. Hanabusa, *Langmuir*, 2003, **19**, 8622–8624; (*b*) J. Seo, J. W. Chung, E.-H. Jo and Y. Park, *Chem. Commun.*, 2008, 2794–2796; (*c*) S. Bhowmik, B. N. Ghosh and K. Rissanen, *Org. Biomol. Chem.*, 2014, **12**, 8836–8839; (*d*) R. Tatikonda, S. Bhowmik, K. Rissanen, M. Haukka and M. Cametti, *Dalton Trans.*, 2016, **45**, 12756–12762.

19 G. R. Whittell, M. D. Hager, U. S. Schubert and I. Manners, *Nat. Mater.*, 2011, **10**, 176–188.

20 (*a*) Q. Liu, Y. Wang, W. Li and L. Wu, *Langmuir*, 2007, **23**, 8217–8223; (*b*) B. N. Ghosh, S. Bhowmik, P. Mal and K. Rissanen, *Chem. Commun.*, 2014, **50**, 734–736; (*c*) M. Xue, Y. Lu, Q. Sun, K. Liu, Z. Liu and P. Sun, *Cryst. Growth Des.*, 2015, **15**, 5360–5367; (*d*) M. Paul, K. Sarkar and P. Dastidar, *Chem. – Eur. J.*, 2015, **21**, 255–268.

21 (*a*) N. N. Adarsh and P. Dastidar, *Cryst. Growth Des.*, 2011, **11**, 328–336; (*b*) L. Sambri, F. Cucinotta, G. D. Paoli, S. Stagni and L. D. Cola, *New J. Chem.*, 2010, **34**, 2093–2096; (*c*) S. Song, A. Song, L. Feng, G. Wei, S. Dong and J. Hao, *Appl. Mater. Interfaces*, 2014, **6**, 18319–18328.

22 (*a*) J. R. Nitschke, *Acc. Chem. Res.*, 2007, **40**, 103–112; (*b*) P. Mal, D. Schultz, K. Beyeh, K. Rissanen and J. R. Nitschke, *Angew. Chem., Int. Ed.*, 2008, **47**, 8297–8301; (*c*) P. Mal, B. Breiner, K. Rissanen and J. R. Nitschke, *Science*, 2009, **324**, 1697–1698; (*d*) W. Meng, B. Breiner, K. Rissanen, J. D. Thoburn, J. K. Clegg and J. R. Nitschke, *Angew. Chem., Int. Ed.*, 2011, **50**, 3479–3483; (*e*) T. K. Ronson, C. Giri, N. K. Beyeh, A. Minkkinen, F. Topić, J. J. Holstein, K. Rissanen and J. R. Nitschke, *Chem. – Eur. J.*, 2013, **19**, 3374–3382; (*f*) C. Giri, F. Topić, P. Mal and K. Rissanen, *Dalton Trans.*, 2014, **43**, 17889–17892; (*g*) A. M. Castilla, W. J. Ramsay and J. R. Nitschke, *Acc. Chem. Res.*, 2014, **47**, 2063–2073; (*h*) J. Roukala, J. Zhu, C. Giri, K. Rissanen, P. Lantto and V.-V. Telkki, *J. Am. Chem. Soc.*, 2015, **137**, 2464–2467; (*i*) C. Giri, F. Topić, M. Cametti and K. Rissanen, *Chem. Sci.*, 2015, **6**, 5712–5718.

23 (*a*) A. Y.-Y. Tam and V. W.-W. Yam, *Chem. Soc. Rev.*, 2013, **42**, 1540; (*b*) W. Fang, X. Liu, Z. Lu and T. Tu, *Chem. Commun.*, 2014, **50**, 3313; (*c*) K. Hong, Y. K. Kwon, J. Ryu, J. Y. Lee, S. H. Kim and K. H. Lee, *Sci. Rep.*, 2016, **6**, 29805; (*d*) Z.-X. Liu, Y. Feng, Z.-Y. Zhao, Z.-C. Yan, Y.-M. He, X.-J. Luo, C.-Y. Liu and Q.-H. Fan, *Chem. – Eur. J.*, 2014, **20**, 533–541.

24 K. Nath, A. Husain and P. Dastidar, *Cryst. Growth Des.*, 2015, **15**, 4635–4645.

25 (*a*) Y. He, Z. Bian, C. Kang, Y. Cheng and L. Gao, *Chem. Commun.*, 2010, **46**, 3532–3534; (*b*) Y. Zhang, B. Zhang, Y. Kuang, Y. Gao, J. Shi, X. X. Zhang and B. Xu, *J. Am. Chem. Soc.*, 2013, **135**, 5008–5011.

26 (*a*) R. Aoyama, H. Sako, M. Amakatsu and M. Yamanaka, *Polym. J.*, 2015, **47**, 136–140; (*b*) P. Wei, X. Yan and F. Huang, *Chem. Soc. Rev.*, 2015, **44**, 815–832.

27 (*a*) S. Butun and N. A. Sahiner, *Polymer*, 2011, **52**, 4834–4840; (*b*) Y. Lu, P. Spyra, Y. Mei, M. Ballauff and A. Pich, *Macromol. Chem. Phys.*, 2007, **208**, 254–261; (*c*) V. Thomas, M. M- Yallapu, B. Sreedhar and S. K. Bajpai, *J. Colloid Interface Sci.*, 2007, **315**, 389–395; (*d*) B. Xia, Q. Cui, F. He and L. Li, *Langmuir*, 2012, **28**, 11188–11194; (*e*) P. Rajamalli, P. Malakar, S. Atta and E. Prasad, *Chem. Commun.*, 2014, **50**, 11023–11025.

28 (*a*) J. Wu, S. Hou, D. Ren and P. T. Mather, *Biomacromolecules*, 2009, **10**, 2686–2693; (*b*) J. Nanda, B. Adhikari, S. Basak and A. Banerjee, *J. Phys. Chem. B*, 2012, **116**, 12235–12244.

29 (*a*) B. Adhikari and A. Banerjee, *Chem. – Eur. J.*, 2010, **16**, 13698–13705; (*b*) M. Eid, *J. Inorg. Organomet. Polym.*, 2011, **21**, 297–301.

30 B. Hu, S. Wang, K. Wang, M. Zhang and S. Yu, *J. Phys. Chem. C*, 2008, **112**, 11169–11174.

31 I. A. Wani, A. Ganguly, J. Ahmed and T. Ahmad, *Mater. Lett.*, 2011, **65**, 520–522.

32 X. Gao, L. Wei, H. Yan and B. Xu, *Mater. Lett.*, 2011, **65**, 2963–2965.

33 (*a*) H. Jia, J. Zeng, W. Song, J. An and B. Zhao, *Thin Solid Films*, 2006, **2**, 281–287; (*b*) P. Kshirsagar, S. S. Sangaru, M. A. Malvindi, L. Martiradonna, R. Cingolani and P. P. Pomp, *Colloids Surf., A*, 2011, **392**, 264–270.

34 M.-O. M. Piepenbrock, N. Clarke and J. W. Steed, *Soft Matter*, 2011, **7**, 2412.

35 S. Bhattacharjee, S. K. Samanta, P. Moitra, K. Pramoda, R. Kumar, S. Bhattacharya and C. N. R. Rao, *Chem. – Eur. J.*, 2015, **21**, 5467–5476.

36 M. Kimura, T. Htanaka, H. Nomoto, J. Takizawa, T. Fukawa, Y. Tatewaki and H. Shirai, *Chem. Mater.*, 2010, **22**, 5732–5738.

37 M. Cametti and Z. Dzolic, *Chem. Commun.*, 2014, **50**, 8273–8286.

38 CCDC 1500637–1500639 contain the supplementary crystallographic data for this paper.

39 (*a*) B. Escuder, M. LLusar and J. F. Miravet, *J. Org. Chem.*, 2006, **71**, 7747–7752; (*b*) Nonappa and E. Kolehmainen, *Soft Matter*, 2016, **12**, 6015–6026; (*c*) Nonappa, M. Lahtinen, B. Behera, E. Kolehmainen and U. Maitra, *Soft Matter*, 2010, **6**, 1748–1757; (*d*) V. Noponen, Nonappa, M. Lahtinen, A. Valkonen, H. Salo, E. Kolehmainen and E. Sievänen, *Soft Matter*, 2010, **6**, 3789–3796; (*e*) Nonappa, D. Saman and E. Kolehmainen, *Magn. Reson. Chem.*, 2015, **53**, 256–260.

40 (*a*) O. V. Dolomanov, A. J. Blake, N. R. Champness, M. Schröder and C. Wilson, *Chem. Commun.*, 2003, 682–683; (*b*) A. R. Biju and M. V. Rajasekharan, *Polyhedron*, 2008, **27**, 2065–2068; (*c*) L.-M. Wang, Y. Wang, Y. Fan, L.-N. Xiao, Y.-Y. Hu, Z.-M. Gao, D.-F. Zheng, X.-B. Cui and J.-Q. Xu, *CrystEngComm*, 2014, **16**, 430–440.

41 (*a*) H. Svobodová, Nonappa, M. Lathinen, Z. Wimmer and E. Kolehmainen, *Soft Matter*, 2012, **8**, 3840–3847.